
¹⁸F-Choline PET/MRI: The Additional Value of PET for MRI-Guided Transrectal Prostate Biopsies

Morand Piert¹, Jeffrey Montgomery², Lakshmi Priya Kunju³, Javed Siddiqui³, Virginia Rogers¹, Thekkelnaycke Rajendiran³, Timothy D. Johnson⁴, Xia Shao¹, and Matthew S. Davenport¹

¹Department of Radiology, University of Michigan, Ann Arbor, Michigan; ²Department of Urology, University of Michigan, Ann Arbor, Michigan; ³Department of Pathology, University of Michigan, Ann Arbor, Michigan; and ⁴Department of Biostatistics, University of Michigan, Ann Arbor, Michigan

We assessed the value of fusion ¹⁸F-fluoromethylcholine (¹⁸F-choline) PET/MRI for image-guided (targeted) prostate biopsies to detect significant prostate cancer (Gleason $\geq 3 + 4$) compared with standard (systematic 12-core) biopsies. **Methods:** Within an ongoing prospective clinical trial, hybrid ¹⁸F-choline PET/CT and multiparametric 3T MRI (mpMRI) of the pelvis were performed in 36 subjects with a rising prostate-specific antigen for known ($n = 15$) or suspected ($n = 21$) prostate cancer before a prostate biopsy procedure. PET and T2-weighted MR volumes of the prostate were spatially registered using commercially available software. Biopsy targets were selected on the basis of visual appearance on MRI and graded as low, intermediate, or high risk for significant disease. Volumes of interest were defined for MR-identified lesions. ¹⁸F-choline uptake measures were obtained from the MR target and a mirrored background volume of interest. The biopsy procedure was performed after registration of real-time transrectal ultrasound with T2-weighted MR and included image-guided cores plus standard cores. Histologic results were determined from standard and targeted biopsy cores as well as prostatectomy specimens ($n = 10$). **Results:** Fifteen subjects were ultimately identified with Gleason $\geq 3 + 4$ prostate cancer, of which targeted biopsy identified significantly more ($n = 12$) than standard biopsies ($n = 5$; $P = 0.002$). A total of 52 lesions were identified by mpMRI (19 low, 18 intermediate, 15 high risk), and mpMRI-assigned risk was a strong predictor of final pathology (area under the curve = 0.81; $P < 0.001$). When the mean ¹⁸F-choline target-to-background ratio was used, the addition of ¹⁸F-choline to mpMRI significantly improved the prediction of Gleason $\geq 3 + 4$ cancers over mpMRI alone (area under the curve = 0.92; $P < 0.001$). **Conclusion:** Fusion PET/MRI transrectal ultrasound image registration for targeted prostate biopsies is clinically feasible and accurate. The addition of ¹⁸F-choline PET to mpMRI improves the identification of significant prostate cancer.

Key Words: ¹⁸F-fluoromethylcholine; molecular imaging; PET/MRI; prostate cancer; targeted prostate biopsy

J Nucl Med 2016; 57:1065–1070

DOI: 10.2967/jnumed.115.170878

Several studies have reported superior identification of significant prostate cancer using image-guided (targeted) prostate biopsies compared with nontargeted standard biopsies. Generally, these approaches use multiparametric (mpMRI) as the primary targeting tool or target after fusion with 3-dimensional (3D) endorectal ultrasound (1,2). Both methodologies rely on the diagnostic advantages of mpMRI to reliably identify and risk-stratify clinically significant prostate cancer. However, mpMRI is not perfect; there is a need to better risk-stratify intermediate- and low-risk targets identified on mpMRI. One potential area of opportunity lies with PET/MRI, in which the multiparametric advantages of MRI can be combined with the functional advantages of PET. The introduction of hybrid PET/MRI scanners promises optimal spatial and temporal registration of PET and MRI data with the added benefit of functional imaging.

It has been shown that increased choline uptake is associated with significant primary prostate cancer (3) and cancers with elevated tumor cell proliferation markers (MIB-1/Ki-67) (4). Although choline uptake is not specific for prostate cancer (i.e., it can be seen in benign prostatic hyperplasia [BPH] (3)), there is evidence that fusion PET/MRI using a derived parameter (quotient of ¹¹C-choline lesion SUV and apparent diffusion coefficient obtained from diffusion-weighted MRI) improves image contrast for the identification of Gleason ≥ 7 disease (5). This superior tissue contrast enhances the association of impeded diffusion with intermediate- and high-risk cancers (6–10).

Here we present an interim analysis of the first registered ongoing prospective diagnostic trial of fusion PET/MRI for targeted prostate biopsies. Imaging included ¹⁸F-choline fusion PET/MRI for the diagnosis of prostate cancer using targeted and standard biopsies. The purpose of our study was to determine whether the addition of ¹⁸F-choline PET/CT augmented the identification of clinically significant prostate cancer over MRI alone.

MATERIALS AND METHODS

Patient Population

We report on the first 36 consecutive subjects of this Health Insurance Portability and Accountability Act–compliant registered ongoing prospective trial (Clinicaltrials.gov identifier NCT01751737). The study was conducted in men with rising prostate-specific antigen values with ($n = 15$) or without ($n = 21$) biopsy-proven, untreated localized adenocarcinoma of the prostate scheduled to undergo a clinically indicated prostate biopsy. Exclusion criteria were as follows: prostate biopsy performed less than 6 wk before imaging, previous external radiation treatment of the pelvis, prior malignancy other than basal or squamous cell skin cancers, active inflammatory bowel disease, and acute prostatitis.

Received Dec. 7, 2015; revision accepted Jan. 29, 2016.

For correspondence or reprints contact: Morand Piert, University of Michigan Health System, Department of Radiology, Division of Nuclear Medicine, University Hospital B1G505C, 1500 E. Medical Center Dr., Ann Arbor, MI 48109-0028.

E-mail: mpiert@umich.edu

Published online Mar. 16, 2016.

COPYRIGHT © 2016 by the Society of Nuclear Medicine and Molecular Imaging, Inc.

The institutional ethics committee approved this protocol. Written informed consent was obtained.

Study participants, 64 ± 5.3 y of age (age range, 56–77 y), underwent 1.7 ± 1.4 (range, 0–6) biopsy procedures before entering the trial (Supplemental Table 1; supplemental materials are available at <http://jnm.snmjournals.org>). The mean time interval from the last biopsy to study enrollment was 21.2 ± 17.7 mo, within a range of 3–96 mo. Prior biopsy results included 12 subjects with Gleason 3 + 3 prostate cancer, 2 with low-volume Gleason 3 + 4 prostate cancer, and 17 with no prior prostate cancer diagnosis. In all cases (including prior outside biopsies), tissue obtained was reviewed by the study pathologist masked to the imaging results. Four subjects did not undergo a prior biopsy. Prostate-specific antigen levels at study entry ranged from 3.0 to 153 ng/mL (mean, 13.8 ± 24.7).

Multisequence MRI

All imaging was performed on the same 3T MR unit (Ingenia; Philips Healthcare) without an endorectal coil using a 16-channel phased array coil.

In vivo MRI pelvis examinations of the prostate gland with and without contrast material was performed before biopsy. The following sequences were acquired: axial 3D T2-weighted (T2w) fast spin echo (FSE) (3D VIEW [Philips Healthcare]; voxel size: $1.0 \times 1.0 \times 1.0$ mm; repetition time, 2,051 ms; echo time, 333 ms; field of view, prostate; number of signal averages [NSA], 2), axial/sagittal/coronal T2w 2-dimensional FSE (voxel size, $0.7 \times 0.9 \times 3.0$ mm; repetition time, 4,758 ms; echo time, 110 ms; field of view, prostate; NSA, 1), axial diffusion-weighted imaging (voxel size, $2.3 \times 2.4 \times 3.0$ mm; NSA, 6; b-factors, 0, 100, and 800 s/mm^2), and axial T1-weighted pre- and dynamic postcontrast 3D spoiled gradient echo with spectral adiabatic inversion recovery fat-saturation (dynamic contrast-enhanced; in-plane voxel size, 0.9×0.9 mm; slice thickness, variable by size of prostate; 53 slices; field of view, prostate; 58 dynamic scans; turbo field echo factor, 25; NSA, 1).

For ex vivo MRI, axial and coronal 3D T2w FSE (3D VIEW; voxel size, $0.75 \times 0.75 \times 0.75$ mm; repetition time, 2,451 ms; echo time, 320 ms; NSA, 3) and axial diffusion-weighted imaging (voxel size, $0.5 \times 0.5 \times 3.0$ mm; NSA, 2; b-factors, 0 and 800 s/mm^2) were acquired.

Imaging was reviewed on a PACS workstation (McKesson). An apparent diffusion coefficient map was reconstructed for all diffusion-weighted imaging sequences, and subtraction imaging was generated for all dynamic contrast-enhanced sequences. Lesions were classified using a 3-point Likert scale corresponding to the 3 (low), 4 (intermediate), and 5 (high) risk scores of a typical 5-point scale by 1 fellowship-trained expert genitourinary radiologist with 5 y of experience interpreting multiparametric prostate MRI. At the time of study conception, the Prostate Imaging—Reporting and Data System (PI-RADS) version 2 (11) was not available and therefore was not used, although Likert scales have been shown to have a diagnostic performance similar to the PI-RADS schema (12,13). Although PI-RADS version 1 was available at the time, it was not sufficiently validated and not generally accepted locally or nationally.

^{18}F -Choline PET/CT

^{18}F -fluoromethylcholine (^{18}F -choline) was synthesized under good-manufacturing-practice (GMP) conditions by reacting dimethylamino ethanol with no-carrier-added ^{18}F -fluoromethyl tosylate. Quality control procedures were undertaken using high-pressure liquid chromatography methods to ensure that radiochemical purity was $\geq 95\%$ (14). MRI and ^{18}F -choline PET/CT were acquired separately within 7 ± 12 d; in many cases ($n = 28$) on the same day (range, 0–44 d). MRI was used for clinical decision making and selection of biopsy targets only. PET/CT was performed on a Biograph TrueV mCT scanner with extended field of view and a 40-channel helical CT (Siemens

Medical Solutions) with an intrinsic axial resolution of 4.1 mm in full width at half maximum and time-of-flight reconstruction (15). After a low-dose CT transmission scan was obtained, a 10-min emission scan of the lower abdomen and pelvis followed 20 min after injection of $233 \pm 8 \text{ MBq}$ of ^{18}F -choline. PET images were reconstructed in a $200 \times 200 \times 56$ matrix resulting in a $4 \times 4 \times 4$ mm voxel dimension. Data were corrected for scatter, random events, and decay. Images were reconstructed using an iterative ordered-subset expectation maximization algorithm (trueX, 3 iterations, 21 subsets) with a 4 mm Gaussian filter utilizing an ultra-low-dose CT (40 effective mAs; 120 keV; slice thickness, 4 mm; pitch, 1) without intravenous or oral contrast for attenuation correction.

Image Registration Tasks and Target Selection

PET data were registered onto 3D T2w MR using commercially available software (MIM Maestro). Registration of in vivo modalities (PET/CT onto T2w MRI) was generally achieved without difficulties. The result of rigid registrations was visually assessed using pelvic bones as landmarks. MRI was performed without endorectal coil, and patients were asked to fully empty their bladder for scanning, which limited deformation of the prostate. If rectal content or bladder filling shifted the position of the prostate, a constrained intensity-based, free-form deformable registration was added to register the prostate on MRI and PET (16). Such registration was possible using the outline of the bladder base and internal prostatic structures (such as BPH nodules) identified on both imaging as landmarks.

Lesion borders were drawn by the radiologists on a T2w 3D sequence to define one or more volumes of interest (VOIs) as biopsy targets. This target VOI was mirrored to the contralateral side of the prostate to create a background VOI for later data analysis. In 1 case (identifier [ID] 36; Supplemental Table 1), the target was located in the midline near the base, requiring a caudal (rather than lateral) shift in the mirrored background VOI to a similar anterior location.

Target T2w MRI and Real-Time 3D Transrectal Ultrasound (TRUS) Registration

The biopsy procedure was performed 16 ± 10 d (range, 3–56 d) after PET/CT imaging using a 3D ultrasound system equipped with a magnetic navigation option (Logiq E9; GE Healthcare). The ultrasound transducer was inserted into the rectum under local anesthesia. TRUS MRI registration requires technical skill and additional time (~ 10 –15 min) for suitable targeting. The 3D T2w MR sequence with embedded target information was loaded into the ultrasound system and rigidly fused with real-time 3D ultrasound. We used a semiautomated 3-point registration system in which at least 3 definable intraprostatic structures (e.g., cysts, BPH nodules) were identified and marked on both MR and endorectal ultrasound images in real-time image space at the time of biopsy to permit rigid registration to occur. We subjectively rated the registration quality (0, no registration; 1, poor; 2, adequate; 3, excellent). Adequate or better registration was achieved in most (28/36) cases. If registration attempts failed, a cognitive registration was attempted by targeting a lesion on ultrasound that appeared to be in the vicinity of the MRI-identified lesion (17,18). After targeted biopsies, standard (systematic 12-core) prostate biopsies using an 18-gauge biopsy needle loaded in a spring-action biopsy device were obtained.

Pathologic Evaluation

Biopsy samples and whole-mount sections after prostatectomy were processed for routine histologic assessment (hematoxylin/eosin stain) using the paraffin-embedding process and 3- μm sections. Each tumor focus was assigned a primary and secondary Gleason grade and staged according to American Joint Committee on Cancer guidelines (19). Final pathology was defined as the highest Gleason score of any cancer detected (per side of the prostate gland) from any (reviewed) tissue (prior biopsy, standard and

targeted biopsy, or—if available—prostatectomy specimen as gold standard). For this study, significant prostate cancer was defined conservatively as any Gleason $\geq 3 + 4$ cancer, including low-volume disease (20).

Registration of T2w Ex Vivo Prostate Specimen onto Pathology

Following a methodology described earlier (21), the prostate specimen underwent a 3T ex vivo MRI scan. The images were the basis for an accurate segmentation of the prostate (Vitrea; Vital Images) for subsequent 3D printing of a plastic mold (Dimension Elite 3D; Stratasys) to support precise sectioning. After complete fixation, the specimen was placed into the custom-built mold for a second high-resolution specimen MRI. Then, the prostate was gross-sectioned within the mold in 3-mm intervals. Volumetric 3-mm stacks of histology sections were then registered onto ex vivo MRI to allow a consistent registration of the ex vivo MRI to pathology (22).

Registration of Pathology onto In Vivo T2w PET/MRI

All foci of prostate cancer, including the dominant index nodule, were outlined by the pathologist on whole-mount hematoxylin/eosin slides and registered back into the ex vivo and in vivo MR and PET image volumes, allowing the retrospective verification of whether in vivo imaging correctly identified all tumor lesions and whether targeted lesions were missed at the time of biopsy.

PET/CT Data Analysis

From mpMRI-defined target and mirrored background VOIs, we calculated the ^{18}F -choline target-to-background ratio (TBR). Five ^{18}F -choline PET parameters (SUV_{max} , SUV_{mean} , $\text{SUV}_{\text{mean}} \times \text{volume}$, $\text{SUV}_{\text{max}} \text{ TBR}$, and $\text{SUV}_{\text{mean}} \text{ TBR}$) were determined for further analysis.

Statistics

Analyses were conducted using the R statistical package (R Foundation for Statistical Computing) (23). Data represent mean \pm SD. We compared the continuity-corrected odds ratio between targeted biopsy and final pathology and standard biopsy and final pathology. The primary outcome measure was detection of Gleason $\geq 3 + 4$ prostate cancer. We used a permutation-based test to address repeated measures within subjects (i.e., targeted biopsy and standard biopsy were obtained in each subject). We permuted within each subject the standard biopsy and targeted biopsy labels and calculated the difference in the odds ratio for these biopsy types (i.e., targeted – standard). This was repeated 10,000 times to estimate the permutation distribution under the null hypothesis of no difference. The observed difference in odds ratios was then compared with this distribution.

To assess the value of mpMRI for the prediction of Gleason $\geq 3 + 4$ prostate cancer, we used a logistic regression model with MRI as the only covariate. To assess the added value of PET to mpMRI, we used a logistic regression model with a variable selection procedure (forward and backward stepwise regression). Of the 5 ^{18}F -choline parameters evaluated, only 1 ^{18}F -choline variable ($\text{SUV}_{\text{mean}} \text{ TBR}$) was selected by stepwise regression together with MRI in the final model. To determine whether this PET-based measure improved identification of Gleason $\geq 3 + 4$ prostate cancer, a likelihood ratio test was performed comparing the model with both MRI and $\text{SUV}_{\text{mean}} \text{ TBR}$ and the model with only MRI. To determine the diagnostic performance of a hypothetical PET/MRI combination, the following rule was applied: IF high-risk lesion on mpMRI OR low- or intermediate-risk lesion on mpMRI AND $\text{SUV}_{\text{mean}} \text{ TBR} > 1.583$ THEN Gleason $\geq 3 + 4$.

Contingency table and receiver-operating-characteristic analyses were performed to determine the value of mpMRI versus PET versus combined PET/MRI assessments. A paired Wilcoxon test was performed to assess the percentage core involvement from targeted versus standard biopsy.

RESULTS

Patient-Based Biopsy Results

Targeted biopsies were obtained from 1 ($n = 20$) or 2 ($n = 16$) mpMRI-identified lesions, with an average of 5.0 ± 3.2 targeted biopsy cores per patient. As shown in the Supplemental Table 1, targeted prostate biopsies on a patient basis resulted in the detection of significantly more Gleason $\geq 3 + 4$ prostate cancer ($n = 12$, permutation based odds ratio = 705.7) compared with nontargeted standard biopsies ($n = 5$, odds ratio = 12.7; $P = 0.002$). In 9 cases, significant prostate cancer was found by targeted biopsies only; in 3 cases only standard biopsies (including 1 prior biopsy) were positive for Gleason $\geq 3 + 4$ disease; in 3 cases, both methods were positive for Gleason $\geq 3 + 4$ disease. Final pathology from prostatectomy ($n = 10$) revealed that image-guided biopsy of a Gleason 3 + 4 prostate cancer missed the target that was correctly identified by mpMRI (ID 26 [Supplemental Table 1]). Targeting increased the maximum percentage biopsy core involvement for any detected cancer to $64\% \pm 26\%$ (range, 30%–100%) compared with $25\% \pm 26\%$ (range, 5%–85%) for standard cores ($P = 0.011$). The number of low-risk cancers (Gleason = 3 + 3) found at standard biopsies was not statistically different from targeted biopsies ($P = 0.49$).

Lesion-Based Results

Fifty-two lesions were identified by mpMRI: 19 low risk, 18 intermediate risk, and 15 high risk. Overall, mpMRI was a strong predictor for significant cancer (odds ratio = 6.29, $P < 0.001$). If only mpMRI-assigned high-risk lesions are considered positive, mpMRI would have resulted in 33 true-negative (TN), 11 true-positive (TP), 4 false-positive (FP), and 4 false-negative (FN) cases (AUC = 0.81). Many of the 15 individual significant cancer lesions found in this patient population were located in the anterior gland ($n = 5$), were close to the apex of the gland ($n = 3$), or were small volume lesions less than 0.5 cm^3 ($n = 7$) (Fig. 1).

We assessed whether the addition of ^{18}F -choline PET/CT would improve the accuracy of mpMRI for the diagnosis of significant cancer. From the following PET parameters tested (lesion SUV_{max} , SUV_{mean} , $\text{SUV}_{\text{mean}} \times \text{lesion volume}$, $\text{SUV}_{\text{max}} \text{ TBR}$, $\text{SUV}_{\text{mean}} \text{ TBR}$), stepwise regression analysis identified the $\text{SUV}_{\text{mean}} \text{ TBR}$ as the most predictive parameter (Supplemental Tables 2A and 2B). Adding the $\text{SUV}_{\text{mean}} \text{ TBR}$ to mpMRI in the statistical model significantly improved the odds to detect Gleason $\geq 3 + 4$ prostate cancer (likelihood ratio = 24.04, $P < 0.001$). The optimal threshold for $\text{SUV}_{\text{mean}} \text{ TBR}$ for mpMRI-identified lesions was determined to be 1.583, which as an individual parameter on all MRI-identified lesions resulted in 33 TN, 12 TP, 4 FP, and 3 FN cases (AUC = 0.92). When $\text{SUV}_{\text{mean}} \text{ TBR}$ was assessed as a combined synthetic criterion (PET/MRI), this improved the prediction for Gleason $\geq 3 + 4$ cancers to 31 TN, 15 TP, 6 FP, and 0 FN (AUC = 0.93).

Pathology results from prostatectomy specimens confirmed the biopsy results for Gleason $\geq 3 + 4$ cancers (combined standard and targeted) in 9 of 10 cases. In 1 discordant case (ID 35 [Supplemental Table 1]), standard and targeted biopsies were negative, but a prior biopsy had shown low-volume Gleason 3 + 4 prostate cancer that was confirmed to be 0.14 cm^3 on whole-mount histology. Given the small lesion volume, it was not surprising that neither mpMRI nor ^{18}F -choline $\text{SUV}_{\text{mean}} \text{ TBR}$ were prospectively or retrospectively abnormal at this location.

In another case (ID 10 [Supplemental Table 1]), a different type of error occurred. The standard biopsy was positive for Gleason 4 + 3 prostate cancer (5% maximum core involvement), but targeted biopsies from 2 targets were negative. Coregistration of histology

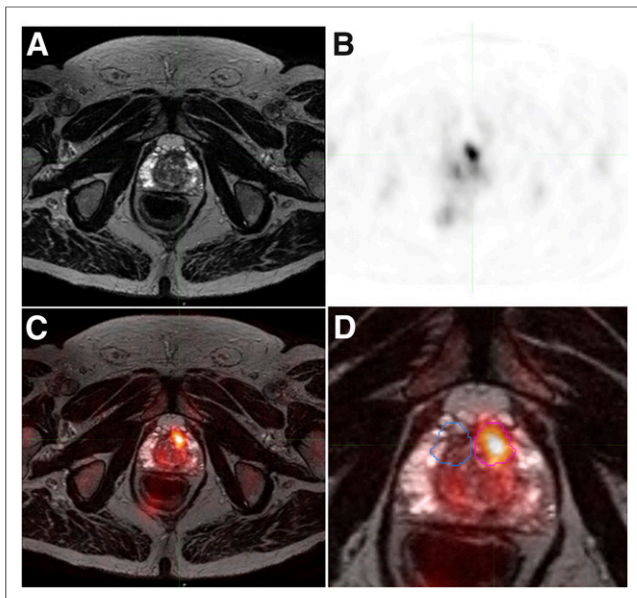


FIGURE 1. Axial 2-dimensional T2w fast spin echo MRI (A), ^{18}F -choline PET (25–30 min after injection; SUV range, 0–12) (B), and fusion PET/MRI (C) showing a 0.68 cm^3 left anterior transitional zone lesion that was confirmed to be Gleason 3 + 4 prostate cancer on targeted biopsy. (D) Magnified view of PET/MRI is displayed with target lesion (magenta) and respective mirrored (blue) background VOIs. This patient (ID 24 [Supplemental Table 1]) underwent 3 prior prostate biopsy procedures without a cancer diagnosis.

with *in vivo* imaging identified that a relatively large (2.1 cm^3) transitional zone cancer was not identifiable by either imaging modality. The lesion presented with heterogeneous signal on T2w images, did not show restricted diffusion, and was undistinguishable from nearby BPH nodules on ^{18}F -choline PET.

DISCUSSION

Our study yielded the following several key findings. Fusion PET/MRI TRUS image registration for targeted prostate biopsies is clinically feasible. The addition of mpMRI-based targeted biopsies to standard biopsies significantly increased the number of identified Gleason $\geq 3 + 4$ lesions. The MRI risk classification was a strong predictor of significant (Gleason $\geq 3 + 4$) disease. The addition of the SUV_{mean} TBR to mpMRI further improved the identification of Gleason $\geq 3 + 4$ cancers over mpMRI alone.

There is now a large body of evidence that transrectal targeted biopsies using MRI TRUS fusion improves the detection rate of significant prostate cancer compared with standard biopsies (1,24). In fact, for the detection of significant disease, transrectal MRI-guided biopsies are as accurate as transperineal biopsies (25), which—until recently—was considered the reference standard for prostate biopsy procedures. Both the PI-RADS system and the generic Likert scales have shown significant positive correlations between the assigned suspicion score and the probability of clinically significant cancer (12,13).

Although mpMRI-guided prostate biopsies appear to be a clear improvement over standard biopsies alone, mpMRI has limitations. A recent study of 235 consecutive patients who underwent mpMRI at 3T with risk-stratification by PI-RADS scoring resulted in an AUC of 0.81 for the detection of clinically significant prostate cancer (26). Our mpMRI data without $^{11}\text{C}/^{18}\text{F}$ -choline PET are similar to these

results. Other recent reports on the detection of significant prostate cancer indicate a high sensitivity but limited specificity (27,28). A larger study including 170 patients undergoing 3T mpMRI with PI-RADS scoring including subsequent pathologic proof (based on prostatectomy) resulted in a sensitivity of 77% and a specificity of 68% for TRUS MRI-guided fusion biopsies regarding the detection of significant disease (13).

Unlike the data supporting the use of mpMRI for clinically significant prostate cancer detection, the reported performance of $^{11}\text{C}/^{18}\text{F}$ -choline PET for primary prostate cancer has been mixed. Results from earlier studies indicated suitable sensitivity but limited specificity for the identification of prostate cancer (29). Because the $^{11}\text{C}/^{18}\text{F}$ -choline uptake of the prostate is often inhomogeneously increased in the central gland, absolute choline uptake measures (SUV_{mean} , SUV_{max}) can be ambiguous as predictors of pathology, and normalization by a suitable background appears to be beneficial (4). We further attribute possible discrepancies in the identification of primary prostate cancer by $^{11}\text{C}/^{18}\text{F}$ -choline PET in part to uncertainties regarding lesion colocalization on imaging compared with pathology due to the relatively poor spatial resolution of PET (21), expected elevated uptake within benign BPH nodules (29,30), and a failure to discriminate between clinically significant versus insignificant prostate cancer (3–5). Our exclusion criteria carefully avoided FP inflammatory lesions (for instance, due to a recent prostate biopsy or acute prostatitis (31)). When ^{11}C -choline PET/CT and MRI have been coregistered with whole-mount histology using *ex vivo* MRI of the prostate specimen, tumor lesions (VOIs) can be defined on the basis of true pathology rather than imaging colocalization (22). This technique has been used with a previous PET/CT scanner generation (effective axial reconstructed PET image resolution between 8.5 and 9 mm), and it was shown that TBR was significantly increased in primary Gleason 4 pattern disease and associated with increased expression of MIB-1/Ki-67, a marker of tumor cell proliferation (4). Without robust coregistration methods, ^{11}C -choline uptake failed to correlate with Gleason scoring and MIB-1/Ki-67 expression in primary prostate cancer (32). More recently, combining ^{18}F -fluoroethylcholine PET/CT and endorectal MRI improved lesion characterization of primary prostate cancer over each modality alone as verified at prostatectomy (3). Also, parametric fusion PET/MRI using the quotient of ^{11}C -choline uptake over apparent diffusion coefficient improved lesion to background contrast of significant cancers to preferentially identify high-risk disease (Gleason $\geq 3 + 4$) (5).

Here we found that both mpMRI and ^{18}F -choline PET/CT using the TBR to mirrored contralateral prostate tissues were strong predictors of Gleason $\geq 3 + 4$ prostate cancer. More importantly, the addition of ^{18}F -choline (as SUV_{mean} TBR) further improved the odds to correctly predict the presence of significant disease over mpMRI alone. When combined as a synthetic PET/MRI parameter, mpMRI with ^{18}F -choline SUV_{mean} TBR improved the predictive value of imaging without any FN cases for MRI-identified lesions (AUC = 0.93). However, Gleason $\geq 3 + 4$ prostate cancer that is low-volume (ID 35 [Supplemental Table 1]), or that presents with uncharacteristic imaging features in unfavorable locations (ID 10 [Supplemental Table 1]), may still escape detection.

We did not test the predictive value of ^{18}F -choline PET/CT independently of mpMRI because we were not attempting to supplant mpMRI with PET/CT. Choline PET/CT without mpMRI is often misleading because ^{18}F -choline uptake can be focally increased in benign tissue, particularly in BPH nodules (3,29), which are better characterized on mpMRI (33). Also, ^{11}C - and ^{18}F -choline PET lack

the tissue contrast and spatial resolution typical of mpMRI. In this study, we assessed ^{18}F -choline PET/CT uptake parameters of mpMRI-identified prostatic lesions; therefore, the highly predictive SUV_{mean} TBR of ^{18}F -choline was not evaluated as an independent PET parameter, nor was that parameter evaluated prospectively without mpMRI information available. Therefore, the improvement in lesion characterization for the diagnosis of significant prostate cancer can be expected only from a combination of both modalities (^{18}F -choline PET/MRI). The benefit of hybrid imaging over fusion PET/MRI as done in this study is 2-fold. First, it eliminates the necessity of additional fusion between methodologies, with minor drawbacks described below. Second and more importantly, only simultaneous hybrid imaging will permit (cross-modality) parametric PET/MR imaging (5) on a voxel-by-voxel basis, which may offer further improvements in characterization of small lesions.

One important limitation of this study is related to the uncertainty of the true histology of targeted lesions, particularly when resulting as benign or low-grade disease due to targeting errors. Also, mpMRI may have entirely missed an existing cancer, which would have precluded a targeted biopsy of that site. We accounted for these errors—at least in part—by combining targeted and standard biopsies. Nonetheless, we have evidence for both types of error as verified in our small subset of patients undergoing prostatectomy.

Multiple registration tasks were required in this study, each of which has task-specific uncertainties. The first registration task (registration of PET onto T2w MRI) was generally performed without difficulties using rigid registration and additional deformable registration when needed. This registration method is clinically applied and well validated for radiation treatment planning of prostate cancer (34). The second registration of the T2w MR (including embedded target information) onto real-time TRUS is more difficult and dependent on many factors such as configuration and size of the prostate gland and patient cooperation. Given that the ultrasound system used in this study required multipoint registration (instead of boundary-based registration), the visibility of intraprostatic features on both ultrasound and MRI was key for successful registration. The accuracy of the TRUS-MRI fusion could therefore only be assessed visually. Despite these issues, our data as well as other studies have shown substantial improvement in the identification of significant prostate cancer by targeted prostate biopsies using TRUS MRI fusion. The third registration task—the registration of a stacked whole-mount histology volume onto coregistered PET/MR using ex vivo prostate MRI—has been previously described (21). This method verified detection of significant cancers missed on targeted biopsy, and it uncovered limitations of imaging to detect significant prostate cancer with unfavorable imaging characteristics.

CONCLUSION

Fusion PET/MRI TRUS image registration for targeted prostate biopsies is clinically feasible and accurate and improves identification of clinically significant prostate cancer over mpMRI alone. If the SUV_{mean} TBR threshold of 1.58 we found in this study is verified in an independent patient population, a combination of mpMRI and ^{18}F -choline PET may be able to challenge the current clinical diagnostic strategy.

DISCLOSURE

The costs of publication of this article were defrayed in part by the payment of page charges. Therefore, and solely to indicate this fact, this article is hereby marked “advertisement” in accordance

with 18 USC section 1734. This study was supported by grants from the Department of Defense (DOD), no. PC110389, and grants NIH/NCI P01CA87634 and P50CA069568. No other potential conflict of interest relevant to this article was reported.

ACKNOWLEDGMENTS

We thank the many dedicated individuals of the Radiology staff and Shawn O’Grady from the University of Michigan 3D lab for his excellent 3D printing.

REFERENCES

- Pinto PA, Chung PH, Rastinehad AR, et al. Magnetic resonance imaging/ultrasound fusion guided prostate biopsy improves cancer detection following transrectal ultrasound biopsy and correlates with multiparametric magnetic resonance imaging. *J Urol*. 2011;186:1281–1285.
- Robertson NL, Emberton M, Moore CM. MRI-targeted prostate biopsy: a review of technique and results. *Nat Rev Urol*. 2013;10:589–597.
- Hartenbach M, Hartenbach S, Bechtloff W, et al. Combined PET/MRI improves diagnostic accuracy in patients with prostate cancer: a prospective diagnostic trial. *Clin Cancer Res*. 2014;20:3244–3253.
- Piert M, Park H, Khan A, et al. Detection of aggressive primary prostate cancer with ^{11}C -choline PET/CT using multimodality fusion techniques. *J Nucl Med*. 2009;50:1585–1593.
- Park H, Wood D, Hussain H, et al. Introducing parametric fusion PET/MRI of primary prostate cancer. *J Nucl Med*. 2012;53:546–551.
- Woodfield CA, Tung GA, Grand DJ, Pezzullo JA, Machan JT, Renzulli JF, II. Diffusion-weighted MRI of peripheral zone prostate cancer: comparison of tumor apparent diffusion coefficient with Gleason score and percentage of tumor on core biopsy. *AJR*. 2010;194:W316–W322.
- Turkbey B, Albert PS, Kurdziel K, Choyke PL. Imaging localized prostate cancer: current approaches and new developments. *AJR*. 2009;192:1471–1480.
- Yoshimitsu K, Kiyoshima K, Irie H, et al. Usefulness of apparent diffusion coefficient map in diagnosing prostate carcinoma: correlation with stepwise histopathology. *J Magn Reson Imaging*. 2008;27:132–139.
- Kim CK, Park BK, Han JJ, Kang TW, Lee HM. Diffusion-weighted imaging of the prostate at 3 T for differentiation of malignant and benign tissue in transition and peripheral zones: preliminary results. *J Comput Assist Tomogr*. 2007;31:449–454.
- Turkbey B, Shah VP, Pang Y, et al. Is apparent diffusion coefficient associated with clinical risk scores for prostate cancers that are visible on 3-T MR images? *Radiology*. 2011;258:488–495.
- Barrett T, Turkbey B, Choyke PL. PI-RADS version 2: what you need to know. *Clin Radiol*. 2015;70:1165–1176.
- Rosenkrantz AB, Kim S, Lim RP, et al. Prostate cancer localization using multiparametric MR imaging: comparison of Prostate Imaging Reporting and Data System (PI-RADS) and Likert scales. *Radiology*. 2013;269:482–492.
- Siddiqui MM, Rais-Bahrami S, Turkbey B, et al. Comparison of MR/ultrasound fusion-guided biopsy with ultrasound-guided biopsy for the diagnosis of prostate cancer. *JAMA*. 2015;313:390–397.
- Rodnick ME, Brooks AF, Hockley BG, Henderson BD, Scott PJ. A fully-automated one-pot synthesis of [^{18}F]fluoromethylcholine with reduced dimethylaminoethanol contamination via [^{18}F]fluoromethyl tosylate. *Appl Radiat Isot*. 2013;78:26–32.
- Jakoby BW, Bercier Y, Conti M, Casey ME, Bendriem B, Townsend DW. Physical and clinical performance of the mCT time-of-flight PET/CT scanner. *Phys Med Biol*. 2011;56:2375–2389.
- Kirby N, Chuang C, Ueda U, Pouliot J. The need for application-based adaptation of deformable image registration. *Med Phys*. 2013;40:011702.
- Cerantola Y, Haberer E, Torres J, et al. Accuracy of cognitive MRI-targeted biopsy in hitting prostate cancer-positive regions of interest. *World J Urol*. 2016;34:75–82.
- Cool DW, Zhang X, Romagnoli C, Izawa JJ, Romano WM, Fenster A. Evaluation of MRI-TRUS fusion versus cognitive registration accuracy for MRI-targeted, TRUS-guided prostate biopsy. *AJR*. 2015;204:83–91.
- Fleming ID, Cooper JS, Henson DE. *AJCC Cancer Staging Manual*. 5th ed. Philadelphia, PA: Lippincott, Raven; 1998.
- Van der Kwast TH, Roobol MJ. Defining the threshold for significant versus insignificant prostate cancer. *Nat Rev Urol*. 2013;10:473–482.

21. Meyer C, Ma B, Kunju LP, Davenport M, Piert M. Challenges in accurate registration of 3-D medical imaging and histopathology in primary prostate cancer. *Eur J Nucl Med Mol Imaging*. 2013;40(suppl 1):S72–S78.
22. Park H, Piert MR, Khan A, et al. Registration methodology for histological sections and in vivo imaging of human prostate. *Acad Radiol*. 2008;15:1027–1039.
23. Ihaka R, Gentleman R. R: a language for data analysis and graphics. *J Comput Graph Stat*. 1996;5:299–314.
24. Moore CM, Robertson NL, Arsanious N, et al. Image-guided prostate biopsy using magnetic resonance imaging-derived targets: a systematic review. *Eur Urol*. 2013;63:125–140.
25. Radtke JP, Kuru TH, Boxler S, et al. Comparative analysis of transperineal template-saturation prostate biopsy versus MRI-targeted biopsy with MRI-US fusion-guidance. *J Urol*. 2015;193:87–94.
26. Schimmöller L, Quentin M, Arsov C, et al. MR-sequences for prostate cancer diagnostics: validation based on the PI-RADS scoring system and targeted MR-guided in-bore biopsy. *Eur Radiol*. 2014;24:2582–2589.
27. Abd-Alazeez M, Ahmed HU, Arya M, et al. The accuracy of multiparametric MRI in men with negative biopsy and elevated PSA level: can it rule out clinically significant prostate cancer? *Urol Oncol*. 2014;32:45.e17–45.e22.
28. Thompson JE, Moses D, Shnier R, et al. Multiparametric magnetic resonance imaging guided diagnostic biopsy detects significant prostate cancer and could reduce unnecessary biopsies and over detection: a prospective study. *J Urol*. 2014;192:67–74.
29. Krause BJ, Souvatzoglou M, Treiber U. Imaging of prostate cancer with PET/CT and radioactively labeled choline derivatives. *Urol Oncol*. 2013;31:427–435.
30. Farsad M, Schiavina R, Castellucci P, et al. Detection and localization of prostate cancer: correlation of ¹¹C-choline PET/CT with histopathologic step-section analysis. *J Nucl Med*. 2005;46:1642–1649.
31. Reske SN, Blumstein NM, Neumaier B, et al. Imaging prostate cancer with ¹¹C-choline PET/CT. *J Nucl Med*. 2006;47:1249–1254.
32. Breeuwsma AJ, Pruim J, Jongen MM, et al. In vivo uptake of [¹¹C]choline does not correlate with cell proliferation in human prostate cancer. *Eur J Nucl Med Mol Imaging*. 2005;32:668–673.
33. Oto A, Kayhan A, Jiang Y, et al. Prostate cancer: differentiation of central gland cancer from benign prostatic hyperplasia by using diffusion-weighted and dynamic contrast-enhanced MR imaging. *Radiology*. 2010;257:715–723.
34. Studenski MT, Gardner SJ, Den RB. Uncertainties encountered in implementation of adaptive planning with in vivo dosimeters. *Radiol Phys Technol*. 2015;8:81–87.